Quantum Phenomena in a Chirped Parametric Anharmonic Oscillator

I. Barth and L. Friedland
Racah Institute of Physics, Hebrew University of Jerusalem, Jerusalem 91904, Israel
(Received 19 February 2014; published 25 July 2014)

Parametric ladder climbing and the quantum saturation of the threshold for the classical parametric autoresonance due to the zero point fluctuations at low temperatures are discussed. The probability for capture into the chirped parametric resonance is found by solving the Schrödinger equation in the energy basis and the associated resonant phase-space dynamics is illustrated via the Wigner distribution. The numerical threshold for capture into the resonance is compared with the classical and quantum theories in different parameter regimes.

DOI: 10.1103/PhysRevLett.113.040403 PACS numbers: 03.65.-w, 42.50.Lc, 05.45.Xt, 85.25.Cp

Parametric resonance is one of the most interesting and frequently used phenomena in classical and quantum dynamics. It occurs when the natural frequency of a system depends on a parameter modulated at twice the natural system's frequency [1–7]. In the well studied stationary case, the modulation frequency is constant. However, in nonlinear systems the stationary parametric amplification is restricted to small amplitudes, since at larger amplitudes the resonance is destroyed due to the nonlinear frequency shift [1]. A robust method to overcome this limitation is to slowly vary the modulation frequency so that the resonance condition is preserved despite the increase of the amplitude of oscillations. This phenomenon is called parametric autoresonance (PAR). The PAR was studied in such classical oscillatory systems as the anharmonic oscillator [8,9], Faraday waves [10,11], and plasmas [12]. But, what are the quantum effects in the chirped parametrically driven system? For example, the classical threshold on the modulation amplitude for transition to PAR becomes infinite when the initial amplitude of the oscillator [12] goes to zero. Can quantum fluctuations modify this result? More generally, what is the quantum-classical correspondence in the system? Similar questions were addressed recently in the direct autoresonance (AR) problem, where instead of parametric modulations, a chirped external driving force was applied [13–18] and two important quantum limits were identified. The first is the saturation of temperature-dependent classical observables at small temperatures due to quantum fluctuations [19,20]. In the second limit, the smooth classical AR dynamics of many simultaneously coupled energy levels transforms into a quantum ladder climbing involving successive two-level Landau-Zener (LZ) transitions [20–24]. This Letter, for the first time, addresses the quantum limits in application to the PAR, i.e., parametric ladder climbing (PLC) and the saturation of the autoresonance threshold due to quantum fluctuations.

The simplest system exhibiting nonlinear parametric resonance is the oscillator governed by the Hamiltonian

$$H = \frac{p^2}{2} + (1 + \varepsilon\cos\varphi)\frac{x^2}{2} + \beta\frac{x^4}{4} \tag{1}$$

(here all variables and parameters are dimensionless). The frequency of the modulation is chirped, $\omega \equiv d\varphi/dt = 2 + \alpha t$, passing the linear resonance at $t = 0$. We expand the wave function of the oscillator, $|\psi\rangle = \sum_n c_n|\psi_n\rangle$, in the energy basis $|\psi_n\rangle$ of the unmodulated Hamiltonian, i.e., $H(\varepsilon = 0)|\psi_n\rangle = E_n|\psi_n\rangle$ and $\langle\psi_k|\psi_n\rangle = \delta_{k,n}$. Then, the dimensionless ($\hbar = 1$) Schrödinger equation is

$$i\frac{dc_n}{dt} = E_n c_n + \frac{\varepsilon}{2}\sum_k c_k\langle\psi_k|\hat{x}^2|\psi_n\rangle\cos\varphi, \tag{2}$$

where for $\beta \ll 1$ the approximate energy levels are [25] $E_n \approx n + \frac{1}{2} + \frac{3}{8}\beta(n^2 + n + \frac{1}{2})$, $n = 0, 1, 2, \ldots$. We also assume weak coupling, $\varepsilon \ll 1$, and, consequently, neglect the nonlinear corrections of order β in the coupling term, $\langle\psi_k|\hat{x}^2|\psi_n\rangle \approx \frac{1}{2}[\sqrt{Q_n}\delta_{k,n-2} + (2n+1)\delta_{k,n} + \sqrt{Q_{n+1}}\delta_{k,n+2}]$, where $Q_n = n(n+1)$. The resulting equation for c_n is

$$i\frac{dc_n}{dt} = E_n c_n + \frac{\varepsilon}{4}[\sqrt{Q_{n-1}}c_{n-2} + (2n+1)c_n + \sqrt{Q_{n+1}}c_{n+2}]\cos\varphi. \tag{3}$$

We have solved Eq. (3) numerically, subject to ground state initial conditions $c_n(t = -10/\sqrt{\alpha}) = \delta_{n,0}$ for two sets of parameters representing the quantum PLC [Figs. 1(a) and 1(c)] and the classical PAR [Figs. 1(b) and 1(d)]. In the first example, $\{\alpha, \beta, \varepsilon\} = \{10^{-6}, 0.01, 0.04\}$ and 40 energy levels are included in simulations. The energy of the system versus the slow time $\tau = \sqrt{\alpha}t$ is shown in Fig. 1(a). One can see that the response of the quantum anharmonic oscillator to the chirped parametric modulation involves successive transitions between even energy levels, i.e., PLC. We define the anharmonicity parameter $P_2 = 3\beta/4\sqrt{\alpha}$ ($P_2 = 10$ in this example) and observe that $n \to n + 2$ transitions occur at times $\tau_n = 4nP_2$, in agreement with the theory below (dashed black line). To our

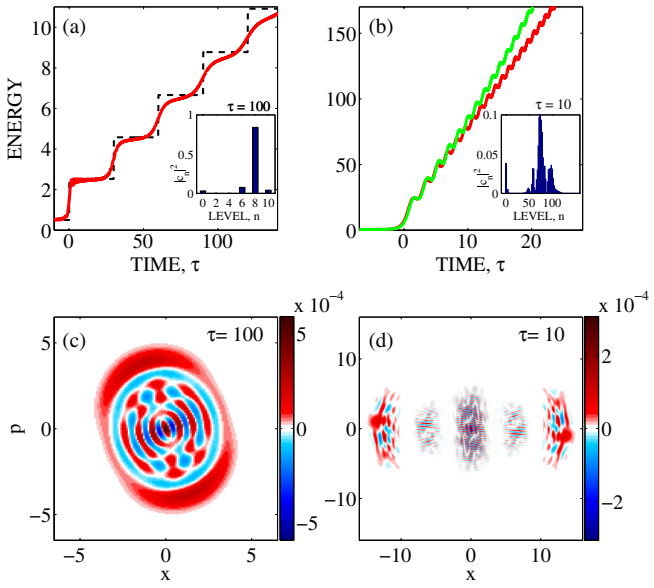

FIG. 1 (color online). The energy of the chirped parametric oscillator in the quantum PLC (a) and the classical PAR (b) regimes versus the slow time τ. In (b), the Schrödinger simulation (lower red line) is compared to the classical solution (upper green line). The inserts are snapshots of the quantum state in the energy basis at given times. The corresponding Wigner distributions are shown in (c) and (d).

knowledge, such a ladder climbing was not observed previously in the chirped parametric oscillator.

The second example [Figs. 1(b) and 1(d)] uses the same initial conditions, but $\{\alpha, \beta, \varepsilon\} = \{10^{-4}, 10^{-3}, 0.04\}$ and 250 levels. Here, $P_2 = 0.075$ corresponds to the classical limit [20,21], where the dynamics involves many levels and the energy grows as expected in the classical PAR [8,12]. We compare this example with the classical simulations, i.e., solve

$$d^2x/dt^2 + (1 + \varepsilon\cos\varphi)x + \beta x^3 = 0 \qquad (4)$$

with the same parameters. The unique characteristic of the classical parametric resonance is the unstable fixed point at zero energy [1]. Therefore, the chirped excitation in the classical case must involve nonzero initial conditions, e.g., a finite energy with random phases, as in Ref. [12], or a thermal distribution of initial conditions, i.e., $f(x_0, u_0) = (2\pi T)^{-1}\exp[-(x_0^2 + u_0^2)/(2T)]$, where $u = dx/dt$. The latter choice is more suitable for studying the classical-quantum correspondence. We use $T = 0.5$ associated with the energy of the quantum mechanical ground state of the unmodulated linearized system. The classical averaged energy over 1000 realizations is plotted in green in Fig. 1(b) showing a good agreement with the quantum simulations. The deviation at large times is due to higher order corrections of the energy levels not included in Eq. (3). This was checked by solving the exact Schrödinger equation for Hamiltonian (1) in the harmonic oscillator basis, which gave an excellent agreement for the energy with the classical results. However, the capture probability (the main observable in the problem) is established at weakly nonlinear times ($\tau < 10$), where the approximate nonlinear model (3) yields greater than 99% accuracy. The fact that the classical results can be reconstructed by solving the quantum equations implies that the correspondence principle is satisfied in the limit of small anharmonicity ($\beta \ll 1$), where many energy levels are coupled simultaneously.

For further illustration, we have calculated the phase-space Wigner distribution [26] in both examples above and show the snapshots at intermediated times in Figs. 1(c) and 1(d). In the first example (PLC), the Wigner distribution at $\tau = 100$ exhibits structure similar to the $n = 8$ level of the quantum ladder, as expected from the energy levels occupation [see Fig. 1(a)]. The deviation from the azimuthally symmetric pure $n = 8$ state is due to the interference with the 15% occupation of the ground and neighboring states [see the inset in Fig. 1(a)]. In the PAR example at $\tau = 10$ in Fig. 1(d), the most populated parts of the phase space are two symmetrically separated resonant phase-space regions of the parametric oscillator, while the interference patterns are seen in the nonresonant regions of phase space. The splitting of the trapped area in phase space into two is explained as a pitchfork bifurcation [9].

One of the important observables of the parametrically chirped oscillator is the probability of capture into resonance. One can define this probability quantum mechanically as the total occupation of resonant levels after the sweeping of the modulation frequency through the linear resonance, or, classically, as the fraction of the initial conditions leading to the phase-locked solution. In the direct AR scenario for a given temperature, the capture probability is a smoothed step function of the driving amplitude ε [27]. The threshold for capture into resonance in this case was defined as the driving parameter ε_{cr} yielding 50% capture probability, i.e., $\varepsilon_{cr} = \varepsilon(P = 0.5)$, while the transition width $\Delta\varepsilon$ was the inverse slope of $P(\varepsilon)$ at $\varepsilon = \varepsilon_{cr}$. ε_{cr} is temperature independent, while $\Delta\varepsilon$ scales as $\sqrt{T}$ [20,27]. Chirped Josephson circuit experiments revealed that at low temperatures, the AR threshold width saturates to a finite value, associated with the ground state of the unperturbed oscillator due to zero point quantum fluctuations [19,20]. This saturation was included in the classical AR theory by introducing an effective temperature $T \to T_{\text{eff}} = (\hbar\omega_0/2k_B)\coth(\hbar\omega_0/2k_BT)$, characterizing the thermal state in the Wigner phase-space representation [20]. In contrast to the direct AR, the low temperature behavior in the PAR has not been studied previously and is discussed next. Numerical simulations of Eqs. (3) show a typical S-shape dependence $P(\varepsilon)$, as in the inset of Fig. 2. Therefore, we define the threshold ε_{cr} for the PAR as $\varepsilon_{cr} = \varepsilon(P = 0.5)$. A classical theory of the PAR was developed in a plasma application, showing that the critical

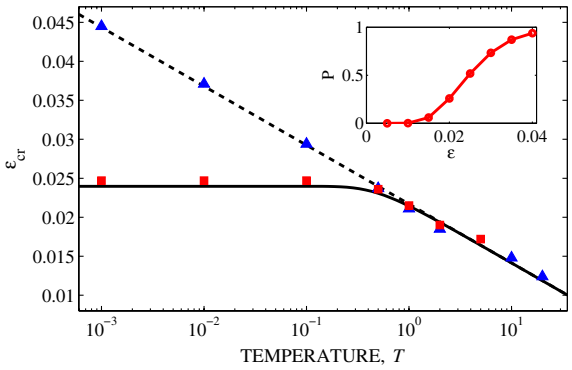

FIG. 2 (color online). The threshold for PAR versus temperature: the classical simulations (blue upward triangle), the theoretical scaling [Eq. (5)] (dashed line), the Schrödinger simulations (red square) showing quantum saturation, and the generalized theory [Eq. (6)] (solid line). Inset: the capture probability $P(\varepsilon)$ at $T = 0.1$ in the quantum simulations.

driving amplitude scales logarithmically with the initial action S_0 of the oscillator, $\varepsilon_{cr} \sim -\ln S_0$ [12]. Therefore, we expect a similar scaling with the initial temperature in our case

$$\varepsilon_{cr}^{PAR}(T) = a - b \ln T. \tag{5}$$

At the same time, we find that the width $\Delta\varepsilon$ of the PAR transition is temperature independent. This result differs significantly from the direct AR, where ε_{cr}^{AR} is temperature independent, while $\Delta\varepsilon \sim \sqrt{T}$ [20]. We verify scaling [Eq. (5)] in numerical simulations of the classical equation of motion [Eq. (4)] subject to random, thermally distributed initial condition [28]. The results are shown in Fig. 2 (blue triangles) for $\alpha = 0.0001$, $\beta = 0.001$. The logarithmic scaling is seen in the semilog figure, while the best-fitted theoretical parameters in this case are $a = 0.021\,7$ and $b = 0.003\,3$. Note that this classical scaling predicts an infinitely large driving amplitude for capture into PAR in the limit of $T \to 0$. This singularity is removed if quantum fluctuations are taken into account. To illustrate this, we solve the Schrödinger equation (3) associated with Hamiltonian (1) using the parameters of the aforementioned classical simulations. The anharmonicity here is small, $P_2 = 0.075 \ll 1$, so many levels are coupled simultaneously and the dynamics is classical, as illustrated in the inset of Fig. 1(b). The numerical quantum results for $\varepsilon_{cr}(T)$ are presented by red squares in Fig. 2, showing a good agreement with the classical simulations for temperatures $T > 0.5$, but exhibiting saturation of the threshold at low temperatures. To include this new effect in the theory, we replace $T \to T_{eff} = \frac{1}{2}\coth(1/T)$ in the classical expression for the threshold (5), i.e.,

$$\varepsilon_{cr}^{PAR}(T) = a - b \ln T_{eff}. \tag{6}$$

This prediction with the coefficients a, b mentioned previously is shown by the solid line in Fig. 2 and agrees with the quantum numerical results at all temperatures. The replacement $T \to T_{eff}$ can be explained via the Wigner phase-space representation. Indeed, the Wigner function of the thermal state of a linearized oscillator is $W(x_0, p_0) = (2\pi T_{eff})^{-1} \exp[-(x_0^2 + p_0^2)/(2T_{eff})]$, while the quantum Liouville equation coincides with the classical Liouville equation in the limit $P_2 \to 0$. Thus, generally, quantum fluctuations in systems exhibiting classical dynamics are taken into account by replacing $T \to T_{eff}$ in the classical theory. Physically, the quantum uncertainty principle imposes a limit on the minimal area of the ground state (at $T = 0$) in phase space, while, classically, it becomes infinitesimally small. As a result, a quantum mechanical upper limit on ε_{cr}^{PAR} is imposed, corresponding to the quantum ground state at $T \to 0$ ($T_{eff} = 0.5$). This completes our discussion of the quantum saturation of the classical PAR at low temperatures. The second quantum limit, where only a few levels are coupled simultaneously and the dynamics becomes that of PLC is discussed next.

For studying the transition between the classical PAR and the quantum PLC regimes, we transform to the rotating frame as follows. First, we define $C_n = c_n e^{iE_n t}$, and rewrite Eq. (3) in the form

$$i\frac{dC_n}{dt} \approx \frac{\varepsilon}{8}\left(\sqrt{Q_{n+1}}C_{n+2}e^{-i(\omega_{n,n+2}t-\varphi)} + \sqrt{Q_{n-1}}C_{n-2}e^{i(\omega_{n-2,n}t-\varphi)}\right), \tag{7}$$

where $\omega_{n,n+2} = E_{n+2} - E_n = 2\text{–}3\beta(2n+3)/4$ and we neglect nonresonant terms (rotating wave approximation). Next, we introduce $B_n = C_n \exp(-i\int \tilde{\Gamma}_n dt)$, where $\tilde{\Gamma}_n = \frac{3}{8}\beta Q_n - \frac{1}{2}n\alpha t$ and $\tau = \sqrt{\alpha}t$. Then, Eq. (7) yields

$$i\frac{dB_n}{d\tau} = \Gamma_n B_n + P_1\left(\sqrt{Q_{n+1}}B_{n+2} + \sqrt{Q_{n-1}}B_{n-2}\right), \tag{8}$$

where $\Gamma_n = \tilde{\Gamma}_n/\sqrt{\alpha} = n/2[P_2(n+1) - \tau]$ and $P_1 = \varepsilon/8\sqrt{\alpha}$, $P_2 = 3\beta/4\sqrt{\alpha}$. We have solved the slow Eqs. (8) numerically, subject to the ground state initial conditions, $B_n(\tau = -10) = \delta_{n,0}$, and calculated the resonant capture probability P (P_1) for different values of the anharmonicity parameter P_2. The numerics of these slow equations is less time consuming, still yielding a good agreement with the solutions of the exact equations (7) (not shown). Similar to the definition of ε_{cr}, we define the threshold modulation parameter $P_1^{cr} = P_1$ $(P = 0.5)$ and show P_1^{cr} in Fig. 3 for different values of the anharmonicity $P_2 \in [0.0035, 7.1]$ (green circles), covering both the classical PAR and the quantum PLC regimes. We also calculate the corresponding classical threshold for different P_2 by solving the classical equations (4) subject to the initial "ground state" temperature $T = 0.5$. The resulting $P_{1,class}^{cr}$ (P_2) is shown in Fig. 3

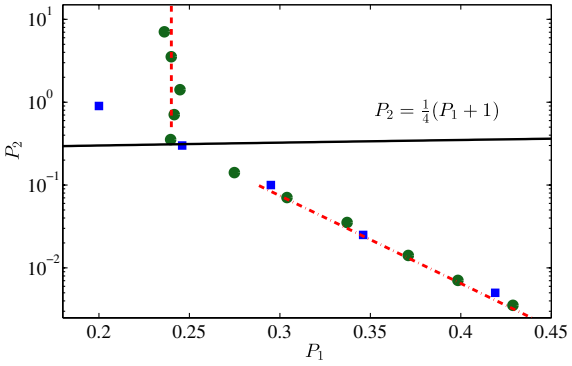

FIG. 3 (color online). The threshold, $P_1^{\rm cr}$ in (P_1, P_2) parameter space: Schrödinger simulations (green circle), PLC theory $P_{1,\rm cr}^{\rm PLC} = 0.237$ (dashed red line), the PAR theory [Eq. (10)] (red dashed dotted line), and the classical simulations (blue square). Black solid line separates the classical PAR and the quantum PLC regimes.

(blue squares) and agrees well with the quantum calculations in the classical regime, $P_2 \ll (P_1 + 1)/4$ (see below).

Next, we seek expressions for $P_1^{\rm cr}$ (P_2) in both the quantum PLC and the classical PAR regimes. In PLC regime, we assume a sufficiently large anharmonicity, such that only two levels are efficiently coupled as the modulation frequency passes the resonance $\omega \approx \omega_{n,n+2}$. In this case, the dynamics is that of successive $n \to n+2$ LZ transitions [23], where the avoided resonant crossing condition occurs when the diagonal terms of the two coupled levels are equal. Therefore, the time of the nth parametric LZ transition is derived by equating the diagonal terms in Eq. (8), i.e., $\Gamma_n = \Gamma_{n+2}$. By solving for τ, one finds that the time of the $n \to n+2$ transition is $\tau_n = 2nP_2$. Therefore, the time interval between successive transitions in PLC limit is $\Delta\tau = \tau_{n+2} - \tau_n = 4P_2$, in agreement with the example in Fig. 1(a) where $P_2 = 10$, so $\Delta\tau = 40$. The typical time of the $0 \to 2$ LZ transition in Eq. (8) in the adiabatic limit is $\Delta\tau_{\rm LZ} = P_1$ and unity in the nonadiabatic limit [29]. Therefore, the condition for well separated successive LZ transitions (i.e., PLC), $\Delta\tau \gg \Delta\tau_{\rm LZ}$, yields $P_2 \gg \frac{1}{4}(P_1 + 1)$. In this limit, the probability of each $n \to n+2$ transition is given by the LZ formula [23] $P_{n\to n+2} = 1 - \exp(-2\pi P_1^2 Q_{n+1})$ and the total probability for capture into PLC starting from the ground state is $P_{\rm total} = \prod_{n=0}^{\infty} P_{n\to n+2}$. Solving $P_{\rm total} = 0.5$ for P_1 yields the threshold for capture into PLC, $P_{1,\rm cr}^{\rm PLC} = 0.237$, where only two first terms in the product are needed for less than 1% accuracy. This prediction is shown in Fig. 3 by a dashed red line and agrees well with the numerical simulations in the quantum PLC regime. In addition, the theoretical separator $P_2 = \frac{1}{4}(P_1 + 1)$ (black solid line) predicts correctly the location of the transition between the quantum PLC and the classical PAR regimes.

Finally, in the PAR regime we write $x = a\cos\theta$, define the slow phase mismatch $\phi = 2\theta - \varphi$ and the rescaled amplitude $A = \sqrt{P_2}a$, employ the single resonance approximation, and average Eq. (4) over the fast phase of the oscillator. This yields [8]

$$\frac{dA}{d\tau} = 2P_1 A\sin\phi; \qquad \frac{d\phi}{d\tau} = A^2 - 2\tau + 4P_1\cos\phi, \quad (9)$$

where, as before, $P_1 = \varepsilon/8\sqrt{\alpha}$, $P_2 = 3\beta/4\sqrt{\alpha}$, $\tau = \sqrt{\alpha}t$, and the initial thermal distribution is $f(A_0) = \sigma^{-2}A_0\exp(-A_0^2/2\sigma^2)$, $\sigma^2 = 0.5P_2T$. Then, the generalized expression for the threshold becomes

$$P_{1,\rm cr}^{\rm PAR}(T) = \kappa_0 - \kappa_1\ln(P_2 T_{\rm eff}), \quad (10)$$

where $\kappa_0 = 0.165$ and $\kappa_1 = 0.41$ are obtained by comparing Eqs. (6) and (10). The numerical results in Fig. 3 agree with this prediction for $T_{\rm eff} = 0.5$ (red dashed-dotted line) in the classical $P_2 \gg \frac{1}{4}(P_1 + 1)$ regime.

The quantum effects in the chirped parametric anharmonic oscillator can be studied in microelectromechanical systems [30] or in Josephson circuit experiments [22,31]. In the latter case, parameters for the low temperature PAR limit can be similar to those in Ref. [22], i.e., the linear frequency $\omega_0/2\pi = f_{0,1} = 6$ GHz, anharmonicity $\beta_r = 0.001$, and chirp rate $\alpha/2\pi = 10$ MHz/ns. In such a system, the dimensionless anharmonicity parameter is $P_2 = 0.15$ in the classical PAR regime (see Fig. 3). For the PAR, we suggest modulating the Josephson critical current, i.e., $I_0 \to I_0[1 + \varepsilon\cos(2\omega_0 t - 0.5\alpha t^2)]$ instead of the external flux $\Phi_{\rm ext}$, as used in the direct AR [see Eq. (2) in the supplemental material of Ref. [22]]. The threshold amplitude [Eq. (10)] of the modulations of I_0 in this example for the initial ground state is $\varepsilon_{cr}^{\rm PAR} = 0.014$, i.e., 1.4% of I_0.

In summary, we have studied the problem of passage through parametric resonance in a quantum anharmonic oscillator and identified the quantum counterpart of the classical PAR, i.e., the quantum PLC. We have developed a theory of PLC and the PAR for thermal initial conditions and found the threshold of capture into resonance in both regimes. We have also studied the transition from PLC to the classical PAR and illustrated both dynamics by the Wigner phase-space distribution. In addition, we have identified the effect of the quantum saturation of the PAR threshold at small temperatures due to zero-point fluctuations. The saturation defines the maximum modulation amplitude needed for efficient PAR excitation. These results pave the way for using PLC and the PAR as robust control tools in quantum electronic or optical systems in such applications as quantum communication and computing. It also seems interesting to extend the study of PLC to quantum systems of many degrees of freedom, such as complex molecules and coupled qubits for controlling different interacting degrees of freedom.

The authors would like to thank Nadav Katz and Yoni Shalibo for constructive discussions. This work was supported by the Israel Science Foundation, Grant No. 451/10.

[1] L. D. Landau, *Mechanics*, 3rd ed. (Oxford, New York, 1976).
[2] R. Di Leonardo, G. Ruocco, J. Leach, M. Padgett, A. Wright, J. Girkin, D. Burnham, and D. McGloin, Phys. Rev. Lett. **99**, 010601 (2007).
[3] P. A. Braun, Theor. Math. Phys. **41**, 1060 (1979).
[4] P. Kinsler and P. D. Drummond, Phys. Rev. A **43**, 6194 (1991).
[5] M. I. Dykman, M. Marthaler, and V. Peano, Phys. Rev. A **83**, 052115 (2011).
[6] T. V. Gevorgyan and G. Yu. Kryuchkyan, Journal of Contemporary Physics (Armenian Ac. Science) **48**, 205 (2013).
[7] P. Krantz, Y. Reshitnyk, W. Wustmann, J. Bylander, S. Gustavsson, W. D. Oliver, T. Duty, V. Shumeiko, and P. Delsing, New J. Phys. **15**, 105002 (2013).
[8] E. Khain and B. Meerson, Phys. Rev. E **64**, 036619 (2001).
[9] O. M. Kiselev and S. G. Glebov, Nonlinear Dynamics **48**, 217 (2007).
[10] M. Assaf and B. Meerson, Phys. Rev. E **72**, 016310 (2005).
[11] O. Ben-David, M. Assaf, J. Fineberg, and B. Meerson, Phys. Rev. Lett. **96**, 154503 (2006).
[12] J. Fajans, E. Gilson, and L. Friedland, Phys. Rev. E **62**, 4131 (2000).
[13] R. Malhotra, Nature (London) **365**, 819 (1993).
[14] G. B. Andresen *et al.* (ALPHA Collaboration), Phys. Rev. Lett. **106**, 025002 (2011).
[15] G. Manfredi and P. A. Hervieux, Appl. Phys. Lett. **91**, 061108 (2007).
[16] J. R. Danielson, T. R. Weber, and C. M. Surko, Phys. Plasmas **13**, 123502 (2006).
[17] K. W. Murch, E. Ginossar, S. J. Weber, R. Vijay, S. M. Girvin, and I. Siddiqi, Phys. Rev. B **86**, 220503(R) (2012).
[18] O. Naaman, J. Aumentado, L. Friedland, J. S. Wurtele, and I. Siddiqi, Phys. Rev. Lett. **101**, 117005 (2008).
[19] K. W. Murch, R. Vijay, I. Barth, O. Naaman, J. Aumentado, L. Friedland, and I. Siddiqi, Nat. Phys. **7**, 105 (2011).
[20] I. Barth, L. Friedland, O. Gat, and A. G. Shagalov, Phys. Rev. A **84**, 013837 (2011).
[21] G. Marcus, L. Friedland, and A. Zigler, Phys. Rev. A **69**, 013407 (2004).
[22] Y. Shalibo, Y. Rofe, I. Barth, L. Friedland, R. Bialczack, J. M. Martinis, and N. Katz, Phys. Rev. Lett. **108**, 037701 (2012).
[23] L. D. Landau, Phys. Z. Sowjetunion **2**, 46 (1932); C. Zener, Proc. R. Soc. A **137**, 696 (1932).
[24] J. H. Kim, W. K. Liu, and J. M. Yuan, J. Chem. Phys. **111**, 216 (1999).
[25] L. Landau and E. M. Lifshitz, *Quantum Mechanics (Non-Relativistic Theory)*, 3rd ed. (Butterworth Heinemann, Oxford, 1977) p. 136.
[26] W. P. Schleich, *Quantum Optics in Phase Space* (Wiley-VCH Verlag, Berlin, 2001), Chap. 3.3, p. 75.
[27] I. Barth, L. Friedland, E. Sarid, and A. G. Shagalov, Phys. Rev. Lett. **103**, 155001 (2009).
[28] The coupling of the driven oscillator to a thermal environment can be modeled by a deterministic oscillator, but with thermally distributed initial conditions.
[29] N. V. Vitanov and B. M. Garraway, Phys. Rev. A **53**, 4288 (1996).
[30] I. Katz, R. Lifshitz, A. Retzker, and R. Straub, New J. Phys. **10**, 125023 (2008).
[31] J. Koch, T. M. Yu, J. Gambetta, A. A. Houck, D. I. Schuster, J. Majer, A. Blais, M. H. Devoret, S. M. Girvin, and R. J. Schoelkopf, Phys. Rev. A **76**, 042319 (2007).